Resonant Brillouin scattering in CuBr

Duy-Phach Vu,* Yasuo Oka,† and Manuel Cardona
Max-Planck-Institut für Festkörperforschung,
Heisenbergstr. 1, 7000 Stuttgart 80, Federal Republic of Germany
(Received 24 December 1980)

We have studied the dispersion of polaritons in CuBr by means of resonant Brillouin scattering. As a result of k-linear terms and exchange coupling the polariton dispersion relations are highly structured. From a theoretical fit we have derived the pertinent exciton parameters and from them the corresponding Luttinger band parameters. The scattering mechanisms invoked for the interpretation of the experiments are piezoelectric scattering and deformation potential scattering. On the basis of independently determined deformation-potential constants it is shown that the deformation-potential scattering suffices to account for the observed scattering efficiencies in piezoelectric forbidden cases. From an analysis of the scattering intensities it is possible, in principle, to determine independently the absolute deformation potentials of the conduction and the valence bands.

INTRODUCTION

The problem of the dispersion of excitons in direct-gap semiconductors with degenerate valence bands is receiving increasing interest both theoretically and experimentally.[1] Since the formal theoretical treatment of Dresselhaus,[2] Baldereschi and Lipari,[3] Kane,[4] Fishman,[5] and most recently Hönerlage *et al.*,[6] have calculated the dispersion of excitons using different approaches. Kane demonstrated that the energy dispersion, for an arbitrary direction in $\vec{k}$ space, results in two bands interpreted as the dispersion of "heavy" and "light" excitons. In his calculation the electron-hole exchange interaction as well as linear terms in k are neglected. Fishman extended Kane's theory by including the so-called short- and long-range exchange interaction. Hönerlage *et al.* applied the general treatment of symmetry-breaking effects on excitons outlined by Cho[7] to CuBr, including the effects arising from the finite exciton momentum $\hbar\vec{k}$. They obtained the exciton dispersion from an invariant expansion of the center-of-mass Hamiltonian in which exchange interactions up to second order in $\vec{k}$ are included.

On the experimental side, the analysis of the optical spectra must take into account the strong interaction between the electromagnetic field and the excitons resulting in coupled states called (excitonic) polaritons.[8] Several techniques have been used for the study of polaritons. Among the most direct ones are two-photon Raman scattering, also called hyper-Raman scattering (HRS),[6,9–11] and resonant Brillouin scattering (RBS).[12] The determination of the polariton dispersion by RBS has been carried out in many different semiconductors such as GaAs,[13] CdS,[14] CdTe,[15] CdSe,[16] ZnSe,[17] ZnTe,[18] and HgI_2.[19] For the zinc-blende-type semiconductors, up to now, the experimental findings are satisfactorily explained by the simple two-band model [GaAs (Ref. (13) and CdTe (Ref. 15)] and by the three-band model [GaAs (Refs. 1 and 13), ZnSe (Ref. 17), and ZnTe (Ref. 18)] which take into account both the heavy and light excitons. In these materials the theory of Fishman and Kane can be used due to a small exchange interaction and a negligible k-linear term. The situation is completely different in the case of CuBr. This zinc-blende-type compound has orbitally degenerate valence bands at $\vec{k} = 0$. The energy scheme of the exciton ground state, at $\vec{k} = 0$, consists of the triplet levels $\Gamma_3 + \Gamma_4$ separated from the "singlet" Γ_5 by $\Delta_{st} = 1.7$ meV (see Ref. 6), the short-range electron-hole exchange interaction. The latter level is further split by the long-range exchange interaction into the longitudinal (Γ_{5L}) and the transverse (Γ_{5T}) states, the energy difference being $\Delta_{LT} = 12.2$ meV (see Ref. 6). The comparison of these splittings with the corresponding ones for GaAs [$\Delta_{st} = 0.1$ meV, $\Delta_{LT} = 0.08$ meV (Ref. 13)] shows the importance of the exchange effect in CuBr. Besides this particular feature, the k-linear term has proved to be the origin of many interesting effects in CuBr.[20–22]

In this paper, we present the experimental determination of the polariton dispersion in CuBr by RBS. This study complements a previous work on CuBr where, by HRS, a small range in $\vec{k}$ space was

covered.[6,22] Since the L-T splitting is large in this material, by RBS we can reach polariton states with wave vectors up to 10^7 cm^{-1} which corresponds to $\frac{1}{5}$ of the distance from the center to the Brillouin-zone edge. Consequently, compared to HRS, which yields extremely accurate experimental results for k up to $\sim 1.5 \times 10^6$ cm^{-1}, more details can be observed in the dispersion at large k in particular, those due to k^2 terms. Our experimental results are well accounted for on the basis of the theory developed by Hönerlage *et al.*[6] from which reliable values of the polariton parameters are deduced.

Our observations also reflect the fact that CuBr is a highly piezoelectric material. The interaction between the excitonic polaritons and the acoustic phonons is dominated by piezoelectric rather than by deformation-potential coupling. From the measured efficiency ratio between these two mechanisms, we are able to deduce an estimate of the corresponding band deformation potentials. Of particular interest is the fact that the *absolute* deformation potentials of valence and conduction bands can, in principle, be obtained.

EXPERIMENTAL CONDITIONS

The single crystals of CuBr used in the experiments were grown by a vapor-phase-transport method in the Laboratoire de Spectroscopie, Strasbourg, France. Three types of surfaces have been studied: the cleaved (110) surface, the (111) natural surface of thin platelets grown under H_2 atmosphere,[23] and the (001) surface obtained by mechanical preparation. The high-symmetry axes for all samples were determined before optical measurements by x-ray analysis.

RBS experiments were performed at low temperature (20, 5, and 2 K) in nearly backscattering configuration. The exciting laser beam made an angle of $\sim 15°$ relative to the normal to the surface at the outside of the crystal and the observations were almost along this normal. Hence, the scattering processes can be assumed to occur inside the crystal along a high-symmetry axis.

The light source was a Stilben-1 dye laser pumped by a uv argon laser. The power density on the sample was several W/cm^2. The spectral width of the laser line was 0.13 meV full width at half maximum (FWHM). Its polarization direction was determined by a Glan prism and a polarization rotator.

The scattered light from the sample went through a polarization filter and was focused on the entrance slit of a double monochromator. The spectra were recorded by means of a photon-counting system and a multichannel analyzer. The resolution of the total setup was 0.13 meV. The precision in the absolute measurement of the incident photon energy was better than 0.1 meV due to simultaneous recording of reference lines from an argon spectral lamp. In the case of strong Brillouin peaks, the shifts relative to the laser line were determined with a precision better than 0.05 meV. In most of the experiments, the counting rate was 10^4 counts per second.

Figure 1 shows the Brillouin spectra observed at 5 K for scattering vectors along the [111] axis. The polarization vectors of the incident and scattered light are both parallel to the [1$\bar{1}$0] axis. The lowest spectrum corresponds to an excitation photon energy, $\hbar\omega_i = 2.9644$ eV, about 1 meV higher than the triplet exciton states, $E(\Gamma_{3,4}) = 2.9633$ eV.[22] Brillouin lines are seen in both Stokes and anti-Stokes sides, overlapping the exciton luminescence. As the laser photon energy increases, the shifts of these lines increase and new lines appear. In the uppermost spectrum, where the excitation energy is higher than the longitudinal level $E(\Gamma_{5L}) = 2.9766$ eV,[22] up to 12 Brillouin lines can be detected on the Stokes side.

Figure 2 shows the spectra obtained for nearly the same exciting photon energies at 2 K with scattering vectors along the [110] direction. The polarizations of incident and scattered light are parallel to the [001] axis. In contrast to the [111] spectra, the Brillouin lines corresponding to small shifts (labeled TA) are stronger than those having large shifts (labeled LA).

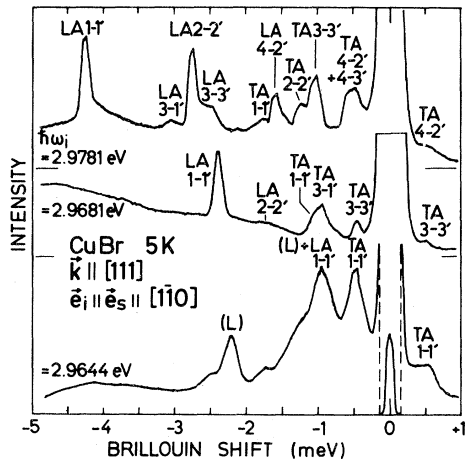

FIG. 1. Resonant Brillouin scattering measured for a (111) surface of CuBr at 5 K in backscattering. The numbers ($1 \rightarrow 1'$) indicate the polariton branches of Fig. 7(b). (L) indicates the luminescence band.

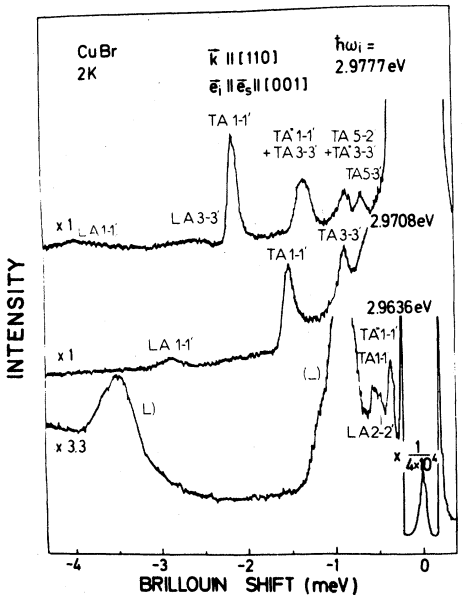

FIG. 2. Resonant Brillouin scattering measured for a (110) surface of CuBr at 2 K in backscattering. The numbers indicate the polariton branches of Fig. 7(a). (L) indicates the luminescence band.

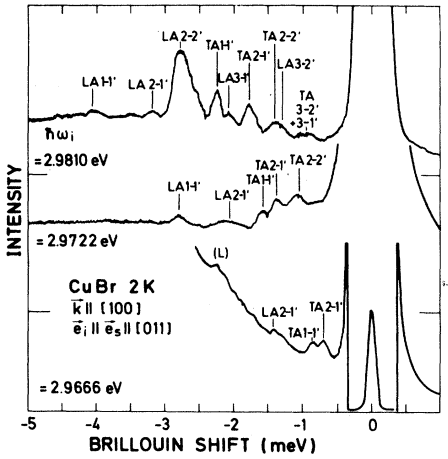

FIG. 3. Resonant Brillouin scattering measured for a (100) surface of CuBr at 2 K in backscattering. The numbers indicate the polariton branches of Fig. 7(b). (L) indicates the luminescence band.

Figure 3 shows the spectra recorded at 2 K in the [100] direction for parallel polarization $\vec{e}_i \| \vec{e}_s \|$ [011]. In this direction, the Brillouin lines are broad and weaker than those observed in the previous directions. This seems due to poor optical quality of the polished surface. It is worth noting that the Brillouin lines were only observable, in this case, after several etchings in pure HBr (piezoelectric coupling does not occur for this face, thus the effect is expected to be weaker, see below).

Figures 4, 5, and 6 show the Brillouin shifts as functions of incident photon energy for [111] direction with $\hat{e}_i \| \hat{e}_s \|$ [$1\bar{1}0$], [110] direction with $\hat{e}_i \| \hat{e}_s \|$ [011], and [100] direction with $\hat{e}_i \| \hat{e}_s \|$ [011], respectively. In the case of the [110] direction, we also studied the Brillouin spectra for $\hat{e}_i \| \hat{e}_s \|$ [$1\bar{1}0$] and $\hat{e}_i \perp \hat{e}_s$ with $\hat{e}_i \| [001]$ or $\| [1\bar{1}0]$. Apart from differences in the relative intensity of the Brillouin peaks, the measured shifts are almost the same as in Fig. 5.

In order to deduce from the experimental data the crystal parameters determining the polariton dispersion, we start from the Hamiltonian acting in the eight-dimensional space of the exciton ground state. This Hamiltonian is constructed by means of an invariant expansion from products of the electron spin operator $\vec{\sigma} = (\sigma_x, \sigma_y, \sigma_z)$ (σ_i being the Pauli spin matrices), the hole angular momentum operator $\vec{J} = (J_x, J_y, J_z)$ (J_i being the angular momentum matrices for $J = \frac{3}{2}$), and the components of the center-of-mass wave vector $\vec{k}$ of the exciton. This Hamiltonian reads[6]

$$H = H_0 + H_1(\vec{k}) + H_s(\vec{k}) , \tag{1}$$

with

$$H_0 = \Delta_0 \underline{1}_e \times \underline{1}_h + \Delta_1 \vec{\sigma} \cdot \vec{J} ,$$

$$H_1(k) = (C_k(k_x\{J_x, J_y^2 - J_z^2\} + \text{c.p.}) + G_1 k^2 \underline{1}_h + G_2[k_x^2(J_x^2 - \tfrac{1}{3}J^2) + \text{c.p.}]$$
$$+ 2G_3(k_y k_z\{J_y, J_z\} + \text{c.p.})) \times 1_e ,$$

$$H_2(\vec{k}) = \delta_1 k^2 \vec{\sigma} \cdot \vec{J} + \delta_2[k_x^2(\sigma_x J_x - \tfrac{1}{3}\vec{\sigma} \cdot \vec{J}) + \text{c.p.}] + 2\delta_3[k_x k_y \tfrac{1}{2}(\sigma_x J_y + \sigma_y J_x) + \text{c.p.}] .$$

1_e, 1_h are 2×2 and 4×4 unity matrices which operate on the space of the electrons and holes respectively, $\{A, B\} = \frac{1}{2}(AB + BA)$, c.p. stands for cyclic permutation. The first term H_0 describes the splitting of the exciton ground state at $\vec{k} = 0$ caused by the isotropic exchange interaction (the anisotropic part has been neglected). This interaction yields the exciton states of symmetry

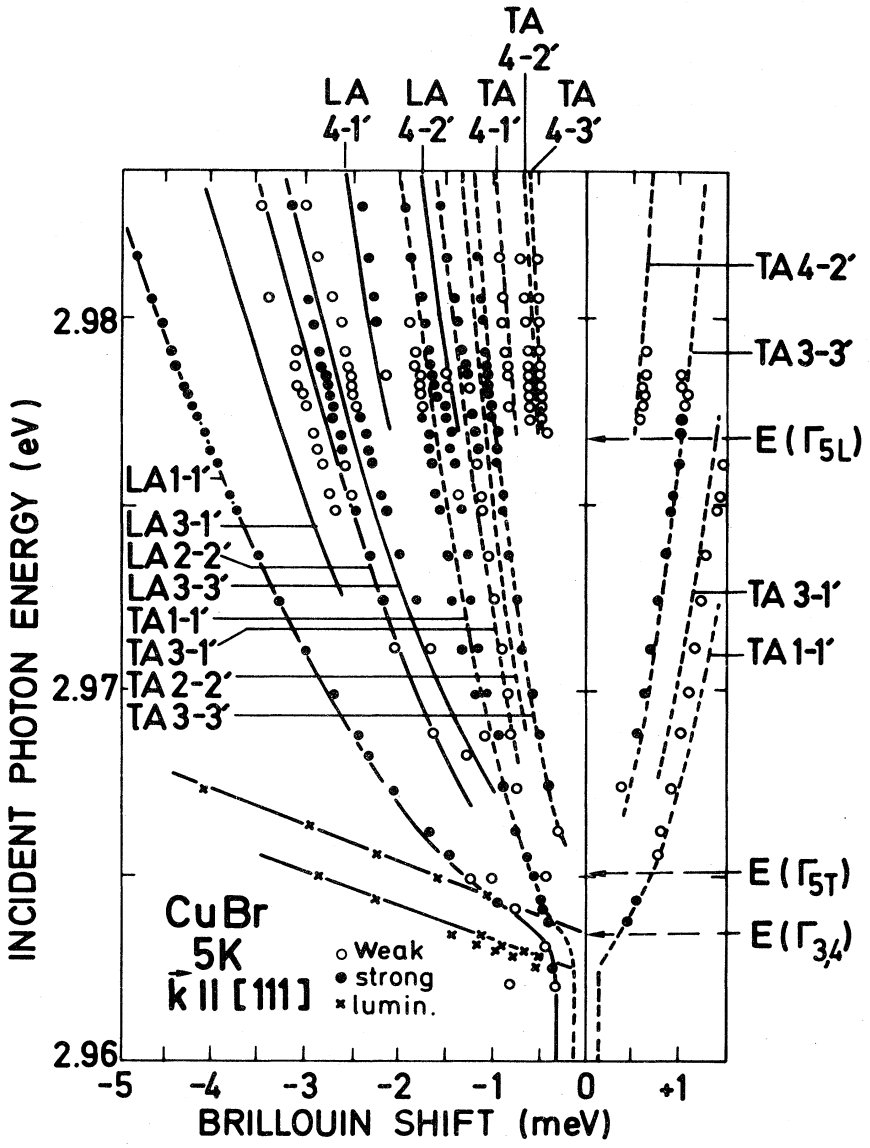

FIG. 4. Experimental and calculated Brillouin shifts for the configuration of Fig. 1.

$\Gamma_3 + \Gamma_4$, Γ_{5T}, and Γ_{5L}. The second term $H_1(\vec{k})$ represents the $\vec{k}$-dependent part which is diagonal with respect to the electron states. It contains terms which are directly derived from corresponding terms of the valence-band effective-mass Hamiltonian.[24,25] C_k is the $\vec{k}$-linear term, G_1 describes the isotropic mass, and G_2 and G_3 indicate the splitting and the directional dependence of the exciton bands. The last term $H_2(\vec{k})$ gives the $\vec{k}$-dependent exchange interaction, where we consider only the leading terms, those bilinear in σ_i and J_i.

By using exciton wave functions which transform as basis functions of the irreducible representations of the group of $\vec{k}$, the matrix representation of H can be reduced into block-diagonal form for the high-symmetry directions. This reduction can be found in Tables III, V, and VI of Ref. 6. The symmetries of the reduced blocks in the notation of the group of the corresponding $\vec{k}$ vector are

For $\vec{k} \| [100]$:

Δ_1 (twice),

Δ_2 (twice),

$\Delta_3 + \Delta_4$ (twice each, degenerate through time reversal),

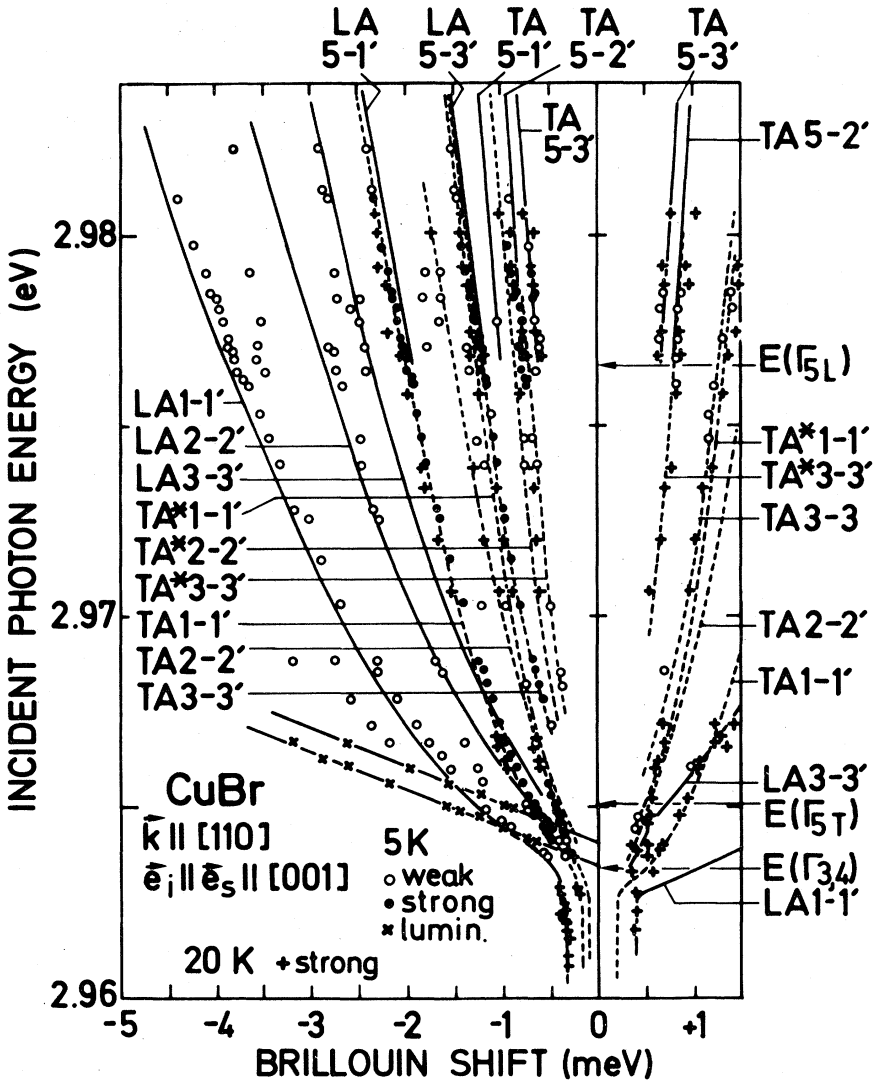

FIG. 5. Experimental and calculated Brillouin shifts for the configuration of Fig. 2.

For $\vec{k}||[111]$:

$$\Lambda_1 \text{ (once)}, \quad \Lambda_2 \text{ (once)}, \quad \Lambda_3 \text{ (three times, twofold degenerate each)}, \tag{2}$$

For $\vec{k}||[110]$:

$$\Sigma_1 \text{ (four times)}, \quad \Sigma_2 \text{ (four times)}.$$

The representations given in Eq. (2) and the corresponding degeneracies account for each k direction for the eight exciton states under consideration. The oscillator strength stems from admixture with the transverse Γ_5 states. ($\Delta_{3,4}$ becomes optically allowed for $\vec{k}||[100]$, Δ_3 for $\vec{k}||[111]$, $\Sigma_1(\hat{e}||[001])$, $\Sigma_2(\hat{e}||[1\bar{1}0])$ for $\vec{k}||[110]$.) The correspondence and continuity relations between the notation of Eq. (2) and that of Figs. 7(a) and 7(b) can be seen in Fig. 2 of Ref. 6. We designate by $\beta(k)$ the oscillator strength of the jth excitons at finite k. Hopfield's equation for the polariton dispersion can be easily extended to the multiple oscillator case[20,6]:

$$\frac{c^2k^2}{\omega^2} = \epsilon_b + \sum_j \frac{4\pi\beta_j(k)E_j(k)^2}{E_j(k)^2 - \hbar^2\omega^2} . \tag{3}$$

ϵ_b is the background dielectric constant. The different solutions $\hbar\omega = E_m(\vec{k})$ of Eq. (3) define the

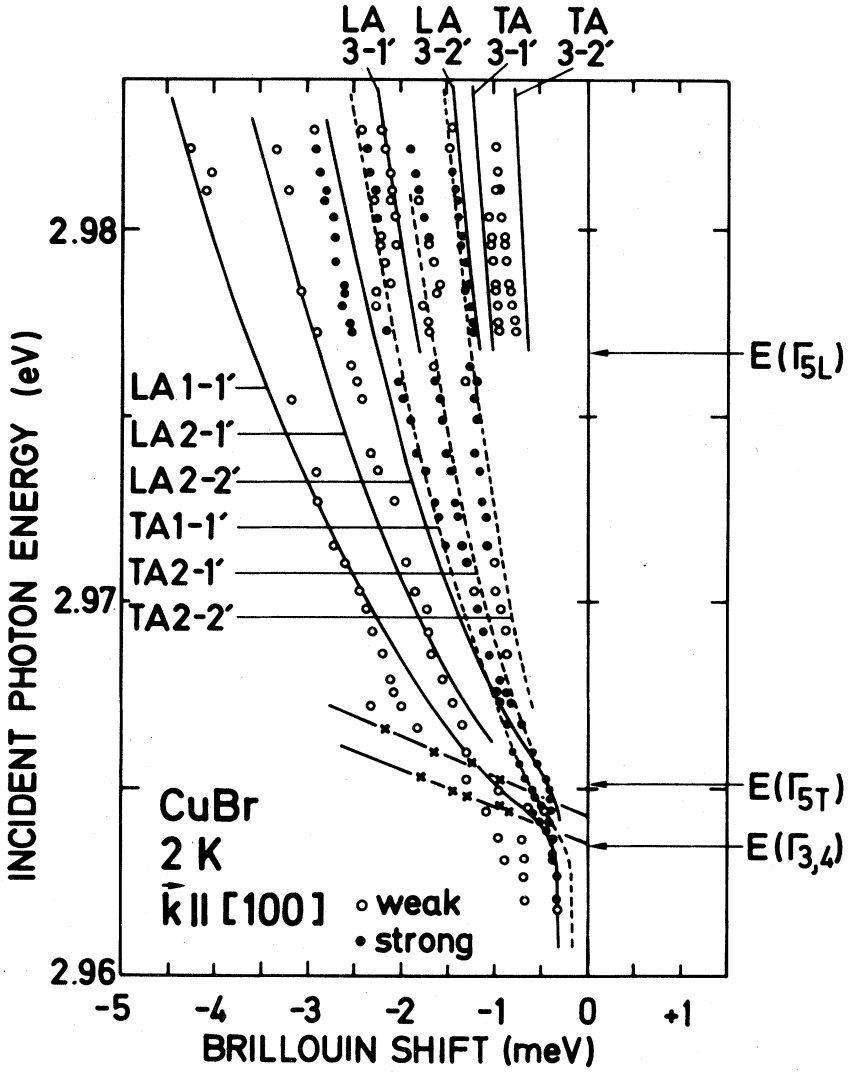

FIG. 6. Experimental and calculated Brillouin shifts for the configuration of Fig. 3.

dispersion of the polariton components.

The scattering of polaritons by acoustic phonons in the backward geometry is governed by the energy and momentum conservation laws

$$E_m(\vec{k}_i) = E_n(\vec{k}_s) \pm \hbar V |\vec{q}| \ , \qquad (4)$$

$$\vec{k}_i = \vec{k}_{s\pm\vec{q}} \ ,$$

where $E_m(\vec{k}_i)$, $E_n(\vec{k}_s)$ are the energy of the incident and scattered polaritons belonging to the mth and nth branches with wave vector $\vec{k}_i$ and $\vec{k}_s$, respectively; $\vec{q}$ is the wave vector of the acoustic phonon and V is the appropriate sound velocity. The $+(-)$ sign corresponds to the Stokes (anti-Stokes) processes.

We have listed in Table I, the sound velocities for different directions of the wave vector $\vec{q}$ and different polarization of the phonons. The notation used in Figs. 1–6 to designate the phonon is also defined in Table I. Using an iterative procedure, we calculate from Eq. (4) the energy shifts for one-phonon scatterings (LA or TA) by the polariton branches resulting from Eq. (3) and fit them to the experimental results. The limits of error quoted for the parameters in Table II were determined in the following way: curve LA $1 \rightarrow 1'$ in Fig. 4 was fitted nearly exactly and curve LA $1 \rightarrow 1'$ in Fig. 5 was fitted as well as possible. Each one of the parameters in Table II was then varied independently and the fit repeated. The limit of error quoted was that

for which a clear worsening of the fits just mentioned could be seen. The LA $1 \rightarrow 1'$ lines were chosen for this procedure as they are the strongest ones observed (see Figs. 1 and 2). No attempt was made to fit the results for the (100) suface (Fig. 6) as the corresponding lines are broad and poorly defined. The curves drawn in Figs. 4, 5, and 6 are the results of the fit. The values thus obtained for the parameters are listed in Table II. The corresponding polariton branches are shown for the three principal k directions in Figs. 7(a) and 7(b). The notation used in Figs. $1-6$ to indicate the polariton branches involved in the scattering processes, refer to the labels 1 to 5 of Figs. 7. The numbers are unprimed for the forward direction and primed for the backward polariton direction. The exciton states which are not coupled with light are not represented in Figs. 7. It is worth noting that Fig. 2 of Ref. 6 displays a blowup of the small-$\vec{k}$ region of Figs. 7(a) and 7(b) (the polariton bottleneck). Our experimental data cannot be fitted without introducing $\vec{k}$-dependent exchange terms. Of these, the most important is the isotropic δ_1 term, the anisotropic part (δ_2, δ_3 terms) is assumed to be negligible.[6] These terms could be the origin of the recent observation in CuCl of a small curvature difference for the longitudinal and transverse exciton bands.[11] However, further studies using several well defined geometries are needed to determine the $\vec{k}$-dependent exchange parameters in CuCl.

As the electron-phonon interaction does not contribute separate terms to the invariant expansion,

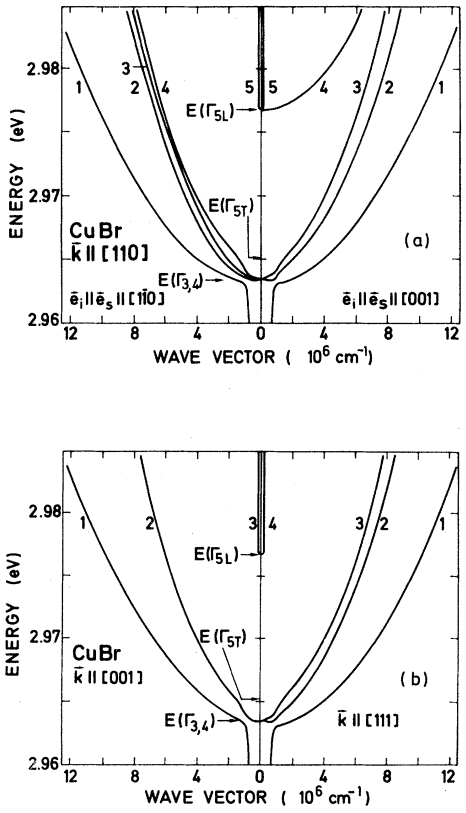

FIG. 7. (a) Polariton curves for $\vec{k}||[110]$. The curves to the right are the components optically active for $\vec{e}||[001]$. Those to the left are active for $\vec{e}||[1\bar{1}0]$. (b) Polariton curves for $\vec{k}||[001]$ (left) and for $\vec{k}||[111]$ (right).

TABLE I. Sound velocities in CuBr. The elastic constants are taken from Ref. 33: $C_{11} = 4.58 \times 10^{10}$, $C_{12} = 3.54 \times 10^{10}$, $C_{44} = 1.39 \times 10^{10}$ N/m^2; $\rho = 5.17 \times 10^3$ kg/m^3.

Phonon wave vector	Polarization	Velocity 10^3 m/s	Notation
[001]	[001]	$(C_{11}/\rho)^{1/2} = 2.98$	LA
	[010] or [100]	$(C_{44}/\rho)^{1/2} = 1.63$	TA
[110]	[110]	$\left[\frac{C_{11}+C_{12}+2C_{44}}{2\rho}\right]^{1/2} = 3.25$	LA
	[001]	$(C_{44}/\rho)^{1/2} = 1.63$	TA
	[1$\bar{1}$0]	$\left[\frac{C_{11}-C_{12}}{2\rho}\right]^{1/2} = 1.0$	TA*
[111]	[111]	$\left[\frac{C_{11}+2C_{12}+4C_{44}}{3\rho}\right]^{1/2} = 3.33$	LA
	[1$\bar{1}$0] or [11$\bar{2}$]	$\left[\frac{C_{11}-C_{12}+C_{44}}{3\rho}\right]^{1/2} = 1.25$	TA

TABLE II. Polariton parameters in CuBr.

	This work	Reference 6
$E(\Gamma_{3,4})$	$=(2963.3 \pm 0.2)$ meV	2962.7 ± 0.1 meV
$E(\Gamma_{5T})$	$=(2965.0 \pm 0.2)$ meV	2964.4 ± 0.2 meV
$E(\Gamma_{5L})$	$=(2976.6 \pm 0.2)$ meV	2976.6 ± 0.2 meV
ϵ_b	$=5.4 \pm 0.2$	5.4 ± 0.2
C_k	$=(50 \pm 6) \times 10^{-8}$ meV cm	$(73 \pm 4) \times 10^{-8}$ meV cm
G_1	$=(0.65 \pm 0.05)\hbar^2/2m_0$	$(0.69)\hbar^2/2m_0$
G_2	$=-(0.10 \pm 0.03)\hbar^2/2m_0$	0
G_3	$=-(0.08 \pm 0.01)\hbar^2/2m_0$	0
δ_1	$=(0.10 \pm 0.01)\hbar^2/2m_0$	$(0.24 \pm 0.02)\hbar^2/2m_0$
δ_2	$=0$	
δ_3	$=0$	

polaron corrections are included in the parameters of the exciton Hamiltonian [Eq. (1)]. The Fröhlich coupling constant in CuBr is calculated to be $\alpha \sim 1$ by taking the electron mass $m_e = 0.21m_0$,[26] the static dielectric constant $\epsilon_0 = 6$ as in Ref. 27, and the high-frequency dielectric constant $\epsilon_\infty = 4$ deduced by using the Lyddane-Sachs-Teller relation from the measured LO- and TO-phonon energies: $\hbar\omega$ (LO) = 20.27 meV, $\hbar\omega$ (TO) = 16.80 meV. Considering that the polaron effect (17%) is not large compared with the experimental uncertainty ($\sim 10\%$) estimated for the parameters of our fit, it is reasonable to assume that we can calculate the Luttinger parameters from the G's by applying relations 9 of Ref. 6 and Kane's theory.[4] The results are listed in Table III, together with the experimental values obtained by HRS (Ref. 6) and by two-photon absorption measurements (TPA)[27], as well as with the theoretical values calculated by Khan.[28] We should mention, however, that the acoustic phonons contributing to the Brillouin scattering are basically similar to those producing the polaron renormalization. It is thus questionable to what extent it is legitimate to use polaron renormalized bands to treat the scattering under consideration.

We first compare our findings with the HRS results also given in Table II. The values obtained for the exciton energies at $k = 0$ and for ϵ_b are in agreement with the corresponding ones determined by HRS. However, for the other parameters, our values are different from those used to fit HRS data. The HRS results are not able to explain our data. We have checked that our dispersion curves cannot be accounted well by the HRS results. Nevertheless the difference in energy between the two sets of dispersion curves is smaller than 0.3 meV at $k = 1.5 \times 10^6$ cm^{-1} which is the maximum value reached by HRS. This difference, however, becomes greater than 5 meV at $k \sim 10^7$ cm^{-1}.

Using the γ_i deduced by TPA along with the exciton energies at $k = 0$, ϵ_b, and C_k determined by our measurements, the polariton dispersion curves show strong anisotropy of the lowest branch (branch 1) with a negative curvature in [110] and [111] directions and a positive curvature in the [001] direction. These types of dispersion definitely cannot explain our experimental observations.

Concerning the theoretical calculations of Khan for the A, B, and, C band parameters,[3,29] the isotropic mass parameter $-2A = \gamma_1$ agrees with our value. The values calculated for γ_2 and γ_3 lie between our experimental ones and those of Ref. 27 (TPA). This fact seems to speak against the correctness of the values $\gamma_2 = \gamma_3 = 0$ of Ref. 6. In comparing band parameters obtained from such different methods as resonant Brillouin scattering, two-photon absorption, and hyper-Raman effect for materials where band renormalizations (exchange, polaron, and polariton) play an important role, one should ask oneself to what extent these renormaliza-

TABLE III. Luttinger parameters in CuBr.

	Our results	HRS (Ref. 6)	TPA (Ref. 27)	Theory (Ref. 28)
γ_1	0.76	0.81 $m_e = 0.21m_0$	0.94 $\gamma'_1 = 5.7$, $m_e = 0.21m_0$	0.78
γ_2	6.7×10^{-2}	0	0.2	0.19
γ_3	5.4×10^{-2}	0	0.56	0.17

tions should be the same for the different experiments. Also, in the Brillouin experiments large values of k are involved, with the positive effect of high accuracy in the parameter determination. One must wonder, however, whether in this case terms of higher order than second order in k should not play an important role. This question cannot be answered at present.

From the Luttinger parameters, we calculate for the three principal directions the heavy- and light-hole masses.[4] They are shown in Table IV. Yu *et al.*[30] and Hönerlage *et al.*[31] have reported an experimental value of $1.4m_0$ for the average hole mass. This is very close to our results. However, as their observations are related to the actual dispersion of the polaritons, exchange effects are included. We also determine the longitudinal exciton masses defined as the curvature of the longitudinal exciton branch. These values are given in the last column of Table IV. They are much smaller than the result $m_L = 10m_0$ reported in Ref. 6.

We discuss now the coupling between excitons and phonons. It is well known that in zinc-blende-type crystals, LA phonons propagating in the [111] direction and TA phonons polarized ||[001] and propagating in the [110] direction carry a longitudinal polarization field induced by the piezoelectric effect. As one can see in Figs. 1 and 2, the most intense Brillouin peaks observed with parallel polarizations ($\vec{e}_i \| \vec{e}_s$) are identified as due to intraband scatterings by the piezoelectrically active phonons. This result shows that piezoelectric (PE) coupling between polariton and phonon, i.e., exciton and phonon, is much more efficient than the deformation-potential (DP) coupling. In Fig. 8, we have plotted the ratio of PE peak intensity to DP peak intensity *for 1-1′ scattering* in [110] direction as a function of the incident photon energy. A theoretical estimate of this ratio is carried out by applying expressions for exciton-phonon matrix elements for PE- and DP-scattering mechanisms given in Ref. 15 [Eqs. (15)–(17)][32]:

$$\frac{I(\mathrm{PE})}{I(\mathrm{DP})} = \frac{16\pi^2 e^2 e_{14}^2}{\epsilon_0^2}\,\frac{V_{\mathrm{DP}}}{V_{\mathrm{PE}}}\,\frac{1}{q^2}\left\{E_c\left[1+\left[\frac{m_h}{m_e+m_h}\right]^2\left[\frac{qa_B}{2}\right]^2\right]^{-2} - E_v\left[1+\left[\frac{m_e}{m_e+m_h}\right]^2\left[\frac{qa_B}{2}\right]^2\right]^{-2}\right\}^2$$
$$\times\left\{\left[1+\left[\frac{m_e}{m_e+m_h}\right]^2\left[\frac{qa_B}{2}\right]^2\right]^{-2} - \left[1+\left[\frac{m_h}{m_e+m_h}\right]^2\left[\frac{qa_B}{2}\right]^2\right]^{-2}\right\}^2, \tag{5}$$

where e_{14} is the piezoelectric constant, q is the energy-dependent phonon wave vector (as $q_{\mathrm{PE}} \sim q_{\mathrm{DP}}$, for simplicity we take $q = q_{\mathrm{DP}}$), E_c and E_v are the deformation potentials for the conduction- and valence-band components of the polariton scattering ($1 \rightarrow 1'$ in our case), and a_B is the exciton Bohr radius. V_{DP} and V_{PE} represent the speed of sound for the deformation-potential and the piezoelectrically coupled phenomena, respectively (see Table I). The most interesting feature of Eq. (5) is the possibility of an independent determination of the *absolute* deformation potentials E_c and E_v from the measured dependence of the $I(\mathrm{PE})/I(\mathrm{DP})$ ratio versus q. The use of an erroneous form for Eq. (5) may account for difficulties in interpreting quantitatively the ratio of intensities reported in the literature.[15]

Taking $e_{14} = 0.27\ \mathrm{C\,m^{-2}}$,[33] $a_B = 17$ Å as calculated from $\epsilon_0 = 6$ and the reduced mass $\mu = (\gamma_1 + \gamma_{1e})^{-1} m_0 = 0.18m_0$, and inserting the appropriate heavy-hole mass and the sound velocities, we obtain a reasonable agreement with the measured ratio by setting the effective exciton deformation potential under static stress $E_c \simeq -E_v = \pm 0.85$ eV. These values, however, depend critically on the number chosen for a_B. If we take $a_B = 10$ Å, for instance, we obtain a best fit with $E_c = \pm 0.15$ eV and $E_v = \pm 0.73$ eV (see Fig.

TABLE IV. Heavy- and light-hole masses and longitudinal masses in CuBr.

k	m_{hh}/m_0	m_{lh}/m_0	m_L/m_0
[001]	$1/(\gamma_1 - 2\gamma_2) = 1.60$	$1/(\gamma_1 + 2\gamma_2) = 1.12$	2.0
[111]	$1/(\gamma_1 - 2\gamma_3) = 1.53$	$1/(\gamma_1 + 2\gamma_3) = 1.15$	2.08
[110]	$1/[\gamma_1 - (3\gamma_3^2 + \gamma_2^2)^{1/2}] = 1.55$	$1/[\gamma_1 + (3\gamma_3^2 + \gamma_2^2)^{1/2}] = 1.14$	2.06

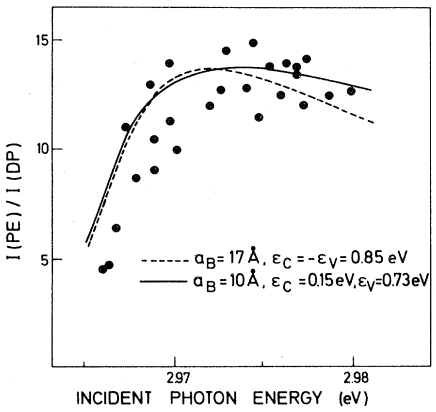

FIG. 8. Ratio of TA to LA $1 \rightarrow 1'$ scattering intensities for the configuration of Fig. 2. The solid and dashed lines are fits with Eq. (5) with the values of E_c, E_v, and a_B, indicated in the figure.

8). These deformation potentials, E_c and E_v, contain two contributions, a hydrostatic and a pure shear one (see the Appendix). For LA phonons the hydrostatic contribution is basically related to the deformation potential of the gap

$$(E_c - E_v)_{\text{hydr}} = a = \frac{dE_0}{d \ln V} , \tag{6}$$

where V is the crystal volume. The deformation potential $a = -0.39$ eV has recently been obtained from measurements of the exciton absorption under hydrostatic pressure in CuBr.[34] The shear contribution affects only the valence bands. It can be expressed in terms of the shear deformation potential b (Ref. 35) for $1 \rightarrow 1'$ scattering. We find (see the Appendix)

$$E = E_c - E_v = a - \frac{b}{4} . \tag{7}$$

Replacing the values $a = -0.39$ eV and $b = -0.42$ eV (obtained by us from the analysis of the data in Ref. 21) we find $E = -0.29$ eV in acceptable agreement with the value $|E| = 0.58$ eV, obtained above for $a_B = 10$ Å, in view of the crudeness of the approximations made. The discrepancy between measured and calculated E's is much larger if we assume $a_B = 17$ Å. These values, however are not to be taken too literally. They are only intended to illustrate the acceptable range of deformation potentials and exciton radii. The LA/TA ratios have also been measured for the (111) face (Fig. 1) for which LA is piezoelectric. In this latter case we find at 2.97 eV $I(\text{LA})/I(\text{TA}) = 2.5$. Using the equivalent of Eq. (5) for this configuration [a factor of $\frac{4}{3}$ must be added to the numerator to take into account the stronger piezoelectric coupling for the (111) face] we find $|E_v| = 0.75$ eV. In this case the deformation-potential scattering occurs for TA phonons and should not contain a hydrostatic part. We find for incident and scattered polarizations parallel to $[1\bar{1}0]$ (the case of Fig. 1):

$$E_v = \frac{1}{2\sqrt{2}} b , \tag{8}$$

and for polarizations parallel to $[11\bar{2}]$:

$$E_v = \frac{b}{2\sqrt{6}} - \frac{d}{3\sqrt{2}} . \tag{9}$$

The deformation potential d has been recently evaluated to be $d = -0.7 \pm 0.1$ eV.[36] Equation (8) yields $E_v = 0.14$ eV, much smaller than the value found experimentally ($E_v = 0.75$ eV). The reason for this anomalously strong TA scattering is unknown. In order to clarify it, measurements for other polarization configurations should be performed.

We would like to mention that for configurations with crossed incident and scattered polarizations piezoelectric scattering is forbidden. Correspondingly we see in these cases a decrease in the strength of the piezoelectric lines by a factor of about 5.

CONCLUSIONS

We have studied by means of resonant Brillouin scattering the dispersion relation of excitonic polaritons in CuBr. From the Brillouin peaks observed for scattering along the [111], [110], and [001] directions, the polariton parameters are determined with high accuracy within the basic assumptions of the Hamiltonian used. The coefficients of the kinetic-energy terms allow us to deduce the Luttinger parameters, and from them, the values of heavy- and light-hole masses corresponding to these high-symmetry directions. The comparison of Brillouin-peak intensities in the case of piezoelectric coupling and in the case of deformation-potential coupling between excitons and phonons yield absolute exciton effective deformation potentials for the conduction and the valence band which are, at least for the [110] scattering direction, in reasonable agreement with independent determinations.

ACKNOWLEDGMENTS

We would like to thank K. Arya, M. Grimsditch, J. B. Grun, A. J. Mattausch, J. C. Merle, R. Ul-

brich, and R. Zeyher for stimulating discussions, and H. Hirt, M. Siemers, and P. Wurster for technical assistance with the measurements. We would also like to thank M. Robinot, M. Joucla, and G. Schwalbach for the preparation of the samples. Special thanks are due to B. Hönerlage and U. Rössler for making their computer program available to us.

APPENDIX

We discuss here the matrix elements of the deformation-potential Hamiltonian between the outer polariton branches $(1 \rightarrow 1')$ for LA phonons with $\vec{k} \| [110]$ and TA phonons with $\vec{k} \| [111]$. These cases are forbidden for piezoelectric coupling. For LA phonons along [110], the eigenvectors of the atomic displacement are

$$u_x = \frac{u}{\sqrt{2}} \exp \frac{ik}{\sqrt{2}}(x+y),$$
$$u_y = \frac{u}{\sqrt{2}} \exp \frac{ik}{\sqrt{2}}(x+y), \qquad \text{(A1)}$$
$$u_z = 0,$$

and the corresponding strain tensor

$$\vec{\varepsilon} = \frac{iku}{2} \begin{bmatrix} 1 & 1 & 0 \\ 1 & 1 & 0 \\ 1 & 1 & 0 \end{bmatrix} = \vec{\varepsilon}_H + \vec{\varepsilon}_u \,, \qquad \text{(A2)}$$

with

$$\vec{\varepsilon}_H = \frac{iku}{3} \begin{bmatrix} 1 & 0 & 0 \\ 0 & 1 & 0 \\ 0 & 0 & 1 \end{bmatrix}$$

and

$$\vec{\varepsilon}_u = \frac{iku}{6} \begin{bmatrix} 1 & 0 & 0 \\ 0 & 1 & 0 \\ 0 & 0 & -2 \end{bmatrix} + \frac{iku}{2} \begin{bmatrix} 0 & 1 & 0 \\ 1 & 0 & 0 \\ 1 & 1 & 0 \end{bmatrix}.$$

The tensor $\vec{\varepsilon}_H$ represents a hydrostatic strain, and hence, the corresponding electron-phonon Hamiltonian will yield as matrix elements straightforward terms proportional to the deformation potential a as discussed above. The pure shear strain $\vec{\varepsilon}_u$ should yield terms containing the deformation potentials b and d of the valence bands.[35] In order to evaluate the matrix elements we must use the eigenvectors obtained by diagonalization of the complete Hamiltonian involving exchange, Coulomb interaction, and linear terms in k. For large values of k the bands $1 \rightarrow 1'$ correspond to the nearly decoupled states $|y'\rangle$, $|z'\rangle$ in the representation of Table V of Ref. 6. These states contain, through exchange coupling, an admixture of the $m_z = \pm\frac{3}{2}$ and $\frac{1}{2}$ valence bands with coefficients which can be found in Ref. 6. The effect of this admixture is to *quench* the b and d coupling. A straightforward evaluation yields

$$\langle 1'_{z'} | H_u | 1_{z'} \rangle = \frac{b}{2} iku \,,$$
$$\langle 1'_{x'} | H_u | 1_{x'} \rangle = -\frac{b}{4} iku \,. \qquad \text{(A3)}$$

The z' component of the 1 polariton branch is polarized along [001] while x' is polarized along $[1\bar{1}0]$. For crossed polarizations one obtains matrix elements involving the deformation potential d.

*On leave from Laboratoire de Spectroscopie, Strasbourg, France. Present address: CNET, B.P. 42, 38240 Meylan, France.
†Present address: Sendai University, Japan.

[1]For a recent review see, U. Rössler, in *Festkörperprobleme Advances in Solid State Physics XIX*, edited by J. Treusch (Pergamon-Vieweg, Braunschweig 1979), p. 77.
[2]G. Dresselhaus, J. Phys. Chem. Solids 1, 14 (1956).
[3]A. Baldereschi and N. O. Lipari, Phys. Rev. Lett. 25, 373 (1970); Phys. Rev. B 3, 439 (1971).
[4]E. O. Kane, Phys. Rev. B 11, 3850 (1975).
[5]G. Fishman, Solid State Commun. 27, 1097 (1978).
[6]B. Hönerlage, U. Rössler, Duy-Plach Vu, A. Bivas, and J. B. Grun, Phys. Rev. B 22, 797 (1980).
[7]K. Cho, Phys. Rev. B 14, 4463 (1976).
[8]J. J. Hopfield, Phys. Rev. 112, 1555 (1958).
[9]T. Itoh and T. Suzuki, J. Phys. Soc. Jpn. 45, 1939 (1978).
[10]B. Hönerlage, A. Bivas, and Duy-Plach Vu, Phys. Rev. Lett. 41, 49 (1978).
[11]T. Mita, K. Sotome, and M. Ueta, Solid State Commun. 33, 1135 (1980).
[12]W. Brenig, R. Zeyher, and J. L. Birman, Phys. Rev. B 6, 4617 (1972).
[13]R. G. Ulbrich and C. Weisbuch, Phys. Rev. Lett. 38, 865 (1977).
[14]G. Winterling and E. Koteles, Solid State Commun. 23, 95 (1977). G. Winterling, E. S. Koteles, and M. Cardona, Phys. Rev. Lett. 39, 1286 (1977); E. S.

Koteles and G. Winterling, *ibid.* 44, 948 (1980).
[15]R. G. Ulbrich and C. Weisbuch, in *Festkörperprobleme (Advances in Solid State Physics)* Vol. XVIII, edited by J. Treusch (Vieweg, Braunschweig, 1978).
[16]C. Herman and P. Y. Yu, Solid State Commun. 28, 313 (1978).
[17]B. Sermage and G. Fishman, Phys. Rev. Lett. 43, 1043 (1979).
[18]Y. Oka and M. Cardona (unpublished).
[19]T. Goto and Y. Nishina, Solid State Commun. 31, 751 (1979).
[20]S. Suga, K. Cho, and B. Bettini, Phys. Rev. B 13, 943 (1976).
[21]C. Wecker, A. Daunois, J. L. Deiss, P. Fiorini, and J. C. Merle, Solid State Commun. 31, 649 (1979).
[22]A. Bivas, Duy-Phach Vu, B. Hönerlage, U. Rössler, and J. B. Grun, Phys. Rev. B 20, 3442 (1979).
[23]T. Goto and M. Ueta, J. Phys. Soc. Jpn. 22, 1123 (1967).
[24]J. M. Luttinger, Phys. Rev. 102, 1030 (1956).
[25]G. Dresselhaus, Phys. Rev. 100, 580 (1955).
[26]P. Fiorini, J. C. Merle, and M. Simon, Phys. Rev. B 22, 4941 (1980).
[27]H. J. Mattausch and Ch. Uihlein, Phys. Status Solidi B 96, 189 (1979).
[28]M. A. Khan, Phys. Status Solidi B 60, 641 (1973).
[29]G. Dresselhaus, A. F. Kip, and C. Kittel, Phys. Rev. 98, 368 (1955).
[30]C. I. Yu, T. Goto, and M. Ueta, J. Phys. Soc. Jpn. 34, 693 (1973).
[31]B. Hönerlage, C. Klingshirn, and J. B. Grun, Phys. Status Solidi B 78, 599 (1976).
[32]Errors in Eqs. (15) and (17a) of Ref. 15 have been corrected. See, A. I. Anselm and I. A. Firsov, Zh. Eksp. Teor. Fiz. 28, 151 (1955) [Sov. Phys.—JETP 1, 139 (1955)].
[33]R. C. Hanson, J. R. Hallberg, and C. Schwab, Appl. Phys. Lett. 21, 490 (1972).
[34]S. Ves. H. Glötzel, H. Overhof, O. K. Andersen, and M. Cardona (unpublished).
[35]M. Cardona, in *Atomic Structure and Properties of Solids,* edited by E. Burstein (Academic, New York, 1972), p. 514.
[36]J. C. Merle and A. Danois (unpublished); S. Ves and M. Cardona (unpublished).